A 10,000-year record of trace metal and metalloid (Cu, Hg, Sb, Pb) deposition in a western Alpine lake (Lake Robert, France): Deciphering local and regional mining contamination

Françoise Elbaz-Poulichet, Stéphane Guédron, Anne-Lise Develle, Remi Freydier, Vincent Perrot, Magali Rossi, Christine Piot, Sophie Delpoux, Pierre Sabatier

A 10,000-year record of trace metal and metalloid (Cu, Hg, Sb, Pb) deposition in a western Alpine lake (Lake Robert, France): deciphering local and regional mining contamination

Françoise Elbaz-Poulichet[1], Stéphane Guédron[2], Develle Anne-Lise[3], Rémi Freydier[1], Vincent Perrot[2], Magali Rossi[3], Christine Piot[4], Sophie Delpoux[1], Pierre Sabatier[3]

[1] Hydrosciences, Univ. Montpellier, CNRS, IRD, Montpellier, France

[2] Univ. Grenoble Alpes, Univ. Savoie Mont Blanc, CNRS, IRD, IFSTTAR, ISTerre, 38000 Grenoble, France

[3] Univ. Grenoble Alpes, Univ. Savoie Mont Blanc, CNRS, EDYTEM, 73000 Chambéry, France

[4] LCME, Univ. Savoie Mont-Blanc, Le Bourget du Lac, France

Keywords: Mercury; Antimony; Lead isotopes; Copper; Alpine Lake; Holocene sediment Record; Bronze Age Pollution

Abstract

Concentrations of trace metals and metalloids (Cu, Hg, Sb, Pb), major elements, stable Pb and C isotope ratios, total organic carbon (TOC), C/N atomic ratios, were analyzed in two sediment cores encompassing 10,000 years of sedimentation sampled in Lake Robert (French Alps).

The results showed that the establishment of a soil cover and vegetation during the Holocene climatic optimum increased Cu and Hg deposition in sediments. Results also enabled reconstruction of the history and local vs regional origins of pollution. During the Bronze Age (1800-1000 BC), Cu mining activities increased Hg and Sb accumulation rates (AR) by a factor of 7 (Hg) and 9 (Sb) compared to pre-Bronze Age values. The rise in Hg AR was equivalent to that of the industrial era highlighting a major local Hg point source not recorded in regional archives. During the Iron Age, Pb pollution was attributed to Sicilian ores whereas during the Roman Empire Pb pollution had the isotopic signature of Spanish Pb ores. During the Medieval period (ca. AD 1200), Pb and Hg pollution was due to the exploitation of the local Ag-Pb mines. Finally, during the industrial era, metal accumulations rates were 90 (Pb), 5 (Hg) and 20 (Sb) times higher than those in the pre-Bronze Age. The isotopic composition of Pb reflected mixed sources including industrial Pb and gasoline Pb. Synchronously, the increase in Sb and Hg pollution is attributed to global and regional atmospheric pollution.

1 Introduction

In their pioneering study of Pb levels in Arctic ice cores, Murozumi et al., (1969), showed that the Northern Hemisphere has been affected by Pb pollution from Roman to modern times. Since that study, long term (pre)-historical metal pollution (mainly Pb, Hg and rarely Cu or other metals) has been identified in Europe in different environmental archives including mires (García-Alix et al., 2013; Küttner et al., 2014; Kylander et al., 2005; Martinez-Cortizas et al., 1999, 1997; Martínez Cortizas et al., 2016; Monna et al., 2011, 2004; Pontevedra-Pombal et al., 2013; De Vleeschouwer et al., 2009; Küttner et al., 2014; Brännvall et al., 1999, 1997; Höppner et al., 2005; Krachler et al., 2008; Roos-Barraclough and Shotyk, 2003; Shotyk et al., 2005, 2004), Posidonia mats (Serrano et al., 2011), estuary sediments (Leblanc et al., 2000), lagoon sediments (Elbaz-Poulichet et al., 2011; Manteca et al., 2017), lake sediments (Chapron et al., 2007; Cooke et al., 2011 and references therein; Renberg et al., 2002, 1994; Thevenon et al., 2011; Schütze et al., 2018) and glacier ice (Preunkert et al., 2019). Long term metal pollution has also been brought to light through the study of lake sediment records in the Andes (Cooke et al., 2011; Guédron et al., 2019) and China (Lee et al., 2008). The main difference between trace metal and metalloid (TMM) records is their respective residence time in the atmosphere, which ranges from approximately 6 months for Hg (Pirrone and Mason, 2009) to a few days or weeks for Pb, Sb and Cu (Krachler et al., 2005; Pacyna, 1987; Sturges and Barrie, 1987), which can result in their dispersal throughout the hemisphere to thousands of kilometers depending on the climatic context. The intensity and location of anthropogenic activities also has a major influence on the

magnitude of TMM records in environmental archives, the highest signals were recorded at the scale of the Northern Hemisphere during the industrial era.

In Europe, mining was already widespread in prehistoric and historic times (Bindler et al., 2009) especially in the Alps where numerous relatively small copper and polymetallic copper bearing deposits have been exploited since the late Neolithic/Early Bronze Age in the Italian (Artioli et al., 2015), Austrian (Höppner et al., 2005) and French (Bourgarit et al., 2008; Carozza, 2010) Alps. Despite the fact most Alpine lake sediments can be used to reconstruct ancient metal pollution (Cooke and Bindler, 2015), there are only few long term records of TMM in these lakes. Yet, as pointed out by (Bindler et al., 2011), such studies are important to establish natural sediment reference conditions for metals and the legacy of long range and local pollution of lakes in Europe. Guyard et al., (2007) reported peak Pb and Cu concentrations during the Roman period (AD 115-330) and Chalcolithic (3770-3870 BP) in sediment layers in Lake Bramant in the western French Alps that reflecting both local and distant mining activities. Later in the same area, Garçon et al., (2012) showed Pb and Ag accumulation peaks in the Lake Blanc d'Huez sediments during the Medieval period, which these authors attributed to exploitation of the Pb-Ag vein in the lake catchment. Thevenon et al., (2011) investigated variations in concentrations of Cu, Cr, Zn, Pb, Hg in Lake Lucerne and Meidsee in the northern Alps in sediment layers encompassing the last 14,000 years. Increased Hg and Pb enrichment compared with crustal values and Pb isotopes provided evidence for the impact of human activities on the lake sediment chemistry during the Chalcolithic (e.g. 3800 BC). Anthropogenic trace metals increased during the Iron Age-Roman period (ca 800 BC to AD 500), the Late Middle Ages (ca AD 1400), after AD 1600 and from the industrial revolution (AD 1850) on, the industrial revolution being

responsible for an exponential increase in metal accumulation in the lakes.

The present study focused on Lake Robert in the western French Alps. It was designed to assess the baseline concentrations and accumulation rates of TMM (Cu, Hg, Sb and Pb) and to decipher the impact of local and regional mining on a remote high-altitude lake.

TMM concentrations and stable Pb isotopes were determined in the layers of two sediment cores covering the entire Holocene. The cores were correlated and dated using ^{14}C.

TMM deposition in lakes is controlled not only by anthropogenic inputs but also by natural factors such as the influx and the sources of organic (OM)/mineral matter (e.g. Schütze et al., 2018) that are dependent on climate-induced environmental changes. In order to better understand variations in lake mineral sedimentation, dry bulk density (DBD), major elements (Ca, Mg, Al, Ti, Si) and total organic carbon (TOC) were determined. In addition, the total organic carbon to nitrogen (C/N) atomic ratio and the C isotopic signature ($\delta^{13}C$) were used to differentiate the source of organic matter in the lake sediments. Indeed, land-derived OM has a higher C/N ratio than 14–20 and negative $\delta^{13}C$ signatures (-24 to -29‰), while phytoplankton and aquatic macrophytes have lower C/N ratios (between 4 and 10) and less negative $\delta^{13}C$ values [-12 to -17 ‰, (Meyers and Teranes, 2001)]. Both the variations of the C/N can thus be used to decipher the autochthonous (in-lake production) and allochthonous (catchment-derived) organic matter (Thevenon et al., 2012).

Water oxygenation is also an important factor controlling metal retention in lake sediments. For example, anoxic conditions in the hypolimnion enhance Cu scavenging by iron sulfides, whereas Cu can be released into solution during aerobic degradation of OM when hypolimnetic oxygenation occurs (e.g. Achterberg et al.,

1997). In oxic water and sediments, Sb is adsorbed/coprecipitated to Fe-Mn oxy(hydro)xides (Belzile et al., 2001). Sb can be released into solution during the reduction of these oxides. In anoxic conditions, Sb sorbs to strongly insoluble Fe sulfides (Chen et al., 2003). Contrary to Cu and Sb, Pb and Hg are generally not subject to diagenetic mobility after deposition (Feyte et al., 2012; Gallon et al., 2004; Rydberg et al., 2008).

Because Mn is more rapidly reduced compared to Fe under anoxic conditions leading to preferential release of Mn (Davison, 1993), higher Fe/Mn ratios indicate lower O_2 concentrations in the water column, whereas lower ratios suggest higher O_2 levels as shown in many lake studies (Brüchmann and Negendank, 2004; Koinig et al., 2003; Loizeau et al., 2001; Naeher et al., 2013; Sabatier et al., 2017). In this study, the Fe/Mn ratio was used as a proxy of water oxygenation at the time of sediment deposition.

2 Study site

The name Lake Robert in fact refers to a set of four endorheic lakes formed after the last glacial maximum retreat in the French Alps at an altitude of 1998 m asl (Fig.1). The lake is frozen from approximately mid-November to mid-May. Fluctuations in the level of the lake caused by seasonal rainfall and snow melt mean the two westernmost lakes are connected for part of the year. The total surface area of the lake is about 0.11 km^2 and water depth ranges from around 4 m in the south-western lake to 12 m in the north-western lakes in April. The Lake Robert watershed is small (1 km^2) and is mainly composed of serpentinized pyroxenites, peridotites, uralitized gabbros and euphotides, post Wurmian till, moraine and coarse scree.

There are no permanent streams and very limited local lithogenic inputs are delivered to the lake sediments.

Old mines are found in the vicinity of the lakes including Challanches mine located 6 km from the lake at 2000 m asl. (Fig.1). From the 18th to the beginning of the 20th century the ore was mainly exploited for its richness in Ag but other TMM were also present. In particular, the presence of numerous Sb containing minerals such as stibnite (Sb_2S_3), cinnabar (HgS) and As, Cu and Ag bearing minerals (i.e., stibarsen (SbAs), dyscrasite (Ag_3Sb) and $Cu_6[Cu_4(Fe,Zn)_2]Sb_4S_{13}$) was reported by (Clavel, 1963; Lacroix, 1893). Old mines have been reported in the Rousses Massif high-altitude (2700-3000 m asl.). The exploitation of Brandes argentiferous Pb mine in this Massif (Fig.1) in the Middle Ages, from AD 1150–1200 to AD 1339, is well documented in written archives (Bailly-Maître, 1996). Several older mines that exploited quartz veins mainly containing chalcopyrite or more rarely copper arsenides and/or antimonides and of superficial formations of copper carbonates in the Bronze Age (2200-1700 BC) have recently been discovered in the vicinity [Fig.1 (Bailly-Maitre and Gonon, 2008; Moulin et al., 2010)].

3 Methods

3.1 Sampling and sample preparation

Two gravity cores ROB15-P5 (115 cm) and ROB15-P6 (110 cm) were collected in the south-western lake (E 5° 54.823'; N 45° 07.968') using an UWITEC gravity corer equipped with a hammer (Fig.1). The two cores were located less than 5 m apart. A hole was drilled in the ice cover to recover sample cores from the sediment at the bottom of the 12-m deep lake in April 2015. In the laboratory, the cores were

split, photographed, and logged in detail, i.e. all the physical sedimentary structures and the vertical succession of facies were recorded. High resolution XRF analysis of Al, Si, Ca, Ti, Mn, Fe, Cu and Pb was performed on the two cores using core scanner. In addition, total organic carbon (TOC) concentrations, ^{13}C, ^{14}C, dry bulk density (DBD), C/N and Hg were determined in core ROB15-P5 and Ca, DBD, Mg, Al, Ti, Si, Fe, Mn, Cu, Sb, Pb and Pb isotopes in discrete samples from core ROB15-P6. The later were chosen to include the major Pb and Cu peaks identified by XRF analysis as well as baseline levels.

3.2 Analysis of ^{14}C

Accelerator mass spectrometers (AMS) were used to measure ^{14}C at the ARTEMIS *Laboratoire de Mesure* 14C (LMC14) at the CEA (Atomic Energy Commission) at Saclay and Poznan Radiocarbon Laboratory. Organic macro-remains were extracted by sieving the sediments. The IntCal13 calibration curve (Reimer et al., 2013) was used for ^{14}C age calibration. The age/depth model was generated using the software-package “clam” (version 3.0.2 R Development Core Team, 2011) (Blaauw, 2010).

As ^{14}C analysis was performed only on the ROB15-P5 core, the ages calculated for this core were correlated the ROB15-P6 core using XRF high resolution data for both cores. The depths in the ROB16-P6 were corrected using the same correlation.

3.3 High resolution XRF geochemical analysis

Variations in concentrations of Al, Si, Ca, Ti, Mn, Fe, Cu and Pb were determined by high resolution XRF analysis on the surfaces of the split sediment cores at 1-mm intervals, using a non-destructive Avaatech core-scanner (see

Supplementary Information (SI)).

3.4 Major elements, dry bulk density (DBD)

Core ROB15-P5 was sampled at 5-mm intervals and dried at 60 °C for 4 days to obtain its DBD. Major elements (Si, Al, Ca, Ti, Fe, Mn) were determined in 31 samples of core ROB15-P6 at the SARM in Nancy (France) using ICP-OES after $LiBO_2$ fusion as described by (Carignan et al., 2001). The variations obtained using XRF geochemical analysis and ICP-OES are in good agreement (SI Fig. S1).

3.5 Total organic carbon (TOC), nitrogen (N) analysis

Total carbon (TC), TOC content were measured in discrete samples from core ROB15-P5 using a Cavity Ring-Down Spectrometer (Picarro, Inc®) coupled with Combustion Module (Costech, Inc®) (CM-CRDS) using analytical methods previously reported in (Guédron et al., 2019), calibration and sample preparation according to (Balslev-Clausen et al., 2013; Paul et al., 2007). More details are given in SI.

Total nitrogen (N) concentrations were obtained by combustion in an automatic C-N analyzer (Elementar VarioMax) on the same samples.

3.6 Cu, Sb, Pb and Pb isotope analysis

High resolution XRF analysis only allows semi quantitative determination of the concentrations of some elements. In order to precisely determine Cu, Sb, Pb concentrations, and to extend the set of elements studied 31 samples were selected in core ROB15-P6. These samples were chosen to better represent the variations observed in the XRF profile. Their Cu, Sb, Pb concentrations and Pb isotopic

composition were determined with the Thermo Scientific® iCAP Q ICP-MS (using the kinetic energy discrimination mode and He as collision gas on the AETE-ISO, OSU OREME platform of the University of Montpellier, France (for more details, see SI).

For Cu and Pb, as shown in SI Fig. S2, the variations obtained using XRF high resolution analysis and ICP-MS are in good agreement.

3.7 Hg analysis

Total Hg concentrations in core ROB15-P5 were determined by atomic absorption spectrophotometry after dry mineralization and gold amalgamation using an automatic mercury analyzer (Altec, Model AMA 254) with a relative precision of ± 10% (Guedron et al., 2009). The analytical quality was insured by analyzing replicate samples (the measurement error was always < 6%), by analyzing certified reference materials (MESS-3 = 90.3 ± 2.8 ng g^{-1}, n=12, 2.3% accuracy). The detection limit ($3SD_{blk}$) was 0.010 µg g^{-1}.

3.8 Enrichment Factors (EF) and TMM Accumulation Rates (AR_T)

TMM concentrations can be influenced by the relative proportions of mineral matter derived from the bedrock and of OM either autochthonous (in lake production) or allochthonous (terrestrial). In order to minimize a possible influence, TMM concentrations (SI Fig. S2) were normalized to Ti, which is a conservative element and a good tracer of minerogenic inputs in lakes of glacial origin (Bajard et al., 2016) and expressed as enrichment factors (EF) relative to mean background (bkg) values calculated as follows:

$XEF=(X/Ti)_{sample}/(X/Ti)_{bkg}$, where X=Cu, Sb, Hg. The bkg values are those observed below 94 cm depth in core ROB15-P6 for Cu, Sb, Pb and 73.5 cm depth in

core ROB15-P5 for Hg.

TMM AR_T was calculated as follows:

XAR_T=(SR)(DBD)([X]) where [X]=Cu, Sb, Pb, Hg concentrations, SR =sedimentation rate, DBD=dry bulk density.

4 Results

4.1 Sedimentology

Based on the description of the sediment and TOC content, the ROB15-P5 core was subdivided into four units (Fig.2):

Unit I (0-6 cm) is composed of olive to grey clayey silt with relatively low OM content (mean TOC= 6%);

Unit II (6-78 cm) is composed of olive silty clay, darker in color between 35 and 60 cm and lighter between 60 and 78 cm with high OM content (mean TOC=8.7%). The variations in color were linked to OM content, which was higher (mean TOC=12%) in the darker facies.

Unit III (78-101 cm) is composed of grey clay to light orange grey clay at the base with submilimetric laminations in the lower part of this unit. The laminations were formed by light grey clay to grey silt alternation with a very low (0.8%) TOC content.

Unit IV (101-115 cm) is composed of a mixture of pebble, gravel and sand with few fine-grained sediments. The contact between Unit III and Unit IV is very abrupt with the presence of a large (5 cm) polished pebble with grooves. Some pebbles are also angular, and their nature is mainly related to the rock present in the watershed.

The ROB15-P6 core has a similar succession of sedimentary Units. Unit I (0-6.5

cm), Unit II (6.5-82 cm) showed the same variations in color, and Unit III (82-110 cm) was also present, whereas Unit IV was absent in this core. Based on this sedimentary description and XRF data, the two cores are precisely correlated.

4.2 Chronostratigraphy

A total of nine radiocarbon analyses were performed on plant macrofossils collected in the top 69 cm (Unit I and Unit II) of the sediment core (Table 1). Unit III and IV were devoid of plant macrofossil remains, hence ^{14}C dating was not possible. Sample SacA42479, at 55 cm, dated to 4900 BP, appeared to be slightly too old, the explanation being that it was probably temporarily stored in the watershed or reworked. Even though this date is not very old compared to the long-term trend, if we retained it, the age model would include short term variations in this part of the core, whereas no variations were observed in other proxies and the calculated fluxes would also be impacted by this age. For these reasons, the age of sample SacA42479 was not included in our age/depth model. We then calculated an age/depth relationship using smooth spline interpolation in the Rcode package "Clam" version 2.2 (Blaauw, 2010). The first 69 cm of the sediment sequence from ROB15-P5 core covered the last 9.98 kyr BP (Fig.2). The mean sedimentation rates estimated from this sediment record at 0.11 mm yr^{-1} varied between 0.28 and 0.03 mm yr^{-1}. The higher sedimentation rate corresponds to the upper part of the core. A major change in the sedimentation rate occurred around 2125±85 BP at 35 cm corresponding to the change in color in Unit II. Above this depth, the mean sedimentation rate was around 0.19 mm yr^{-1} and below this depth, around 0.053 mm yr^{-1} (Fig. 2). In the ROB15-P5 core, sediment accumulation rates varied between 2.10^{-7} g m^{-2} yr^{-1} and 1.310^{-8} g m^{-2} yr^{-1} and presented the same variations as the

sedimentation rates, except in the older part of the core due to higher density of the sediment. If we extrapolate the age/depth model to the base of Unit II we obtain an age of 11,090 ± 440 BC. The sedimentation rate in the lower part of Unit II was probably higher than that in relation to more terrigenous inputs (Fig.3), so the base of this unit probably corresponds to the beginning of the Holocene and Unit III to the late glacial period. During this period - at least at the beginning - a small glacier was probably present in the watershed as suggested by the clay to silt lamination at the base of the Unit. The sedimentation rate in Unit III was probably higher than during the Holocene, as evidenced by more terrigenous content. Even though we cannot precisely date the transition between Unit III and Unit IV, Unit IV probably corresponds to moraine deposits before the glacial retreat in this part of the Alps and the lake formation.

Even though the stratigraphy made it possible to distinguish four Units, TMM analysis was performed in Unit I, II and III only when the lake was present. For core ROB15-P6, the two deepest sediment levels of Unit III could not be dated due to absence of plant macrofossils and were consequently attributed arbitrary ages.

The chronology in the upper part of Unit I is not well constrained as we did not measure short-lived radionuclides, but we assume that the base of Unit I corresponds to the beginning of the construction of ski resorts in the watershed in the middle of the 20th century.

4.3 Major elements and TOC

The sediment cores contained significant proportions of minerogenic elements as indicated by the mean average concentrations of Al (4.6±0.6%), Fe (2.6±0.6%), Ti and Mn (in the thousand and hundred µg g^{-1} range, respectively). As expected in a

catchment devoid of carbonated rocks, the Ca content was low (0.6±0,1%) but higher Mg concentrations (4.0±1.1%) were encountered. As shown in Fig. 3 and in SI Fig. S1, concentrations of Al, Ti, Fe and Mn were high in Unit III (prior to 10,800 BC). In Unit II, the concentrations then decreased down to 49 cm depth (around 2400 BC) and except for Mn and Ca, peak concentrations were generally identified at 38 cm depth (around 720 BC). Two other peak concentrations of all elements were observed at 15.5 cm depth (around AD 1340) in Unit 2 and at 4.5 cm depth concentrations were maximum at 4.5 cm depth (around AD 1890) in Unit 1.

In Unit III, the Fe/Mn ratio was relatively high (0.81≤ Fe/Mn≤0.97 compared to that observed at the basis of Unit II between 54 and 65 cm depth (between 3130 and 6020 BC) (around 0.64). The ratio then increased substantially to reach a maximum of 0.78 at 37 cm depth (around 500 BC). From 34 cm depth (AD 20) to the upper core level, Fe/Mn ratios varied in a small range between 0.66 and 0.71

With a mean concentration of 24±2%, silica was the main component of sediment cores. In Unit III, concentrations were relatively high, ranging from 24% to 26%. In Unit II, the concentrations decreased to 20% at 47 and 52 cm depth (2815 and 2080 BC) (Fig. 3), then concentrations increased and relatively high values (up to 27%) were measured at depths of 9 and 28.5 cm (AD 645 and 1656). Unit I generally displayed lower concentrations (23% to 24%) than those observed in the top sediment levels of Unit II.

In addition to silica, OM is also an important component of particulate matter. TOC was relatively low (0.8%) in Unit III. The concentrations then increased, and a broad peak with values reaching 15.2% was observed at 49 cm depth (around 2400 BC) (Fig.3). Subsequently, a general decreasing trend was observed with a minimum value of 5% at the base of Unit I (AD 1850).

The C/N values varied in a narrow range (9.3-15.6), with an average value of 12.3±1.9). In Unit III and at the base of Unit II, the C/N values were around 9.6. Like TOC, C/N values then increased to a maximum of 16 at 61.5 cm depth (around 4680 BC) and remained above 14 until 46 cm depth (around 1800 BC). The ratios then decreased towards the surface reaching a minimum value of 9.3 at 17.5 cm depth (around AD 1270). In Unit I the C/N ratios ranged from 9.9 to 12.

$\delta^{13}C$ values also remained within a narrow range (-27.9 ± 1.3 ‰). The highest values up to 25.5 were observed in Unit II, after which values decreased again to reach a minimum (-29.7‰) at 27 cm depth (around 5770 BC). Values tended then to increase slightly but remained below 27‰. In Unit I higher values (26.5-26.9‰) were observed.

4.4 TMM concentrations and total accumulation rates (AR_T)

CuEF (Fig. 4) increased regularly to reach maximum (3.9) at 52 cm depth (around 2815 BC) followed by a decreasing trend with a small shoulder at 45 cm depth (around 1790 BC). A minimum value (0.76) was reached at the top of Unit II. In Unit I no enrichment of Cu was observed and CuEF values remained around 1. Comparatively high $CuAR_T$ (up to 690 µg m^{-2} yr^{-1}) were observed in Unit III (Fig. 4). In Unit II, a large but lower peak was observed between 42 and 62 cm depth (1350 to 5000 BC), whereas the highest accumulation rates (up to 1743 µg m^{-2} yr^{-1}) were recorded in Unit I.

From 49 cm to 65 cm depth (from around 2370 to 6020 BC), SbEF ranged from 0.39 to 0.59. (Fig. 4). From 49 cm depth, values increased strongly to reach a maximum of 3.6 4 at 42 cm depth (around 1350 BC), after which EF decreased with three comparatively smaller peaks at 36.1 cm depth (320 BC) (SbEF=1.97). From

this depth up to the top of the core SbEF did not indicate Sb enrichment compared to background values.

The variations in $SbAR_T$ generally resembled those of SbEF (Fig. 4) except in Unit I. In Unit III, $SbAR_T$ was low (mean= 3.4±0.5 µg m^{-2} yr^{-1}, displaying minor variations between 49 and 76 cm depth (2370 and 9600 cal BC). As concentration, $SbAR_T$ displayed a peak (26.3 µg m^{-2} yr^{-1}, 7 times higher than the mean natural flux) at 42 cm depth (around 1350 BC). In the two upper levels of Unit I corresponding to the 20^{th} century AD, high flux values (56 and 29 µg m^{-2} yr^{-1}, 16 and 8 times the mean natural flux) were observed.

HgEF gently increase from 73.5 cm depth (around 8900 cal BC) up to 57.5 cm depth (around 3730 BC) where HgEF values reached a plateau around 12 (Fig. 4). From 47.5 cm depth (around 2015 BC) HgEFincreased sharply to reach maximum EF values (54) at 46 cm depth (1800 BC). HgEF then decreased but remained high (HgEF>4.43). In the uppermost sediment level dated to AD 1997, HgEF was 7.91, which is 7 times lower than the maximum observed in Unit II. Between 67 and 76 cm depth (from around 10,600 to 6350 BC) $HgAR_T$ varied narrowly (mean=0.23±0.06 µg m^{-2} yr^{-1}) (Fig.4). Variations in $HgAR_T$ resembled those of HgEF below 144 cm depth (around 500 cal BC) with a sharp maximum at 6.67 µg m^{-2} yr^{-1} at 46 cm depth (around 1800 BC). This flux is comparable to the present-day flux. Above this depth, two additional small peaks appeared at 36 cm depth (320 BC) ($HgAR_T$= 2 µg m^{-2} yr^{-1}) and between 17 and 24 cm depth (AD 935 to 1300) ($HgAR_T$= 3.90 µg m^{-2} yr^{-1}). From the top of Unit II (8.5 cm depth) and up to the surface a marked increase in fluxes was also observed with values reaching 6 µg m^{-2} $yr^{-}1$ at 5.5 cm depth. The value at the surface, 5.1 µg m^{-2} yr^{-1}, was slightly lower than that observed at 46 cm depth but in the same order of magnitude.

From 65 cm depth (around 6020 BC) until 49 cm depth (around 2370 BC), PbEF (Fig. 4) varied little with values around 1 implying no Pb enrichment relative to background values. From 49 cm depth (around 2370 BC) PbEF started to increase. Four peaks were observed one at 47 cm depth (2080 BC) (EF=3.6), one at 36 cm depth (320 BC) (EF=20.7), another at 19 cm depth (AD 1215) (EF=8.9) and finally at the surface of the core (EF=8.9).

The variations in $PbAR_T$ paralleled those of PbEF (r^2=0.83, except in Unit I (Fig.4). From the bottom of the core to 49 cm depth (2370 BC), $PbAR_T$ varied smoothly between 11 and 21 µg m^{-2} yr^{-1}. The highest flux (294 µg m^{-2} yr^{-1}) was observed at 36 cm depth (around 320 BC). The flux in the top of the core was comparatively lower (119 µg m^{-2} yr^{-1}).

4.5 Lead isotopes

In Unit II and III until 65 cm depth (around 6020 BC), $^{206}Pb/^{207}Pb$ ratios (Fig. 5) were high (mean±1s=1.202±0.003). Between 52 and 62 cm depth (5000 to 2815 BC) slightly lower $^{206}Pb/^{207}Pb$ values (1.190±0.004) were recorded. Then, although highly variable, $^{206}Pb/^{207}Pb$ ratios showed a decreasing trend and their distribution mirrored that of PbEF. Low $^{206}Pb/^{207}Pb$ ratios ($^{206}Pb/^{207}Pb$=1.1881) were observed at 47 cm depth (around 2080 BC), between 35 and 37 cm depth (140 and 500 BC) ($^{206}Pb/^{207}Pb$=1.178), and between 7 and 25 cm depth (AD 880 to 1790) ($1.179 \leq {}^{206}Pb/^{207}Pb \leq 1.182$). In Unit I, $^{206}Pb/^{207}Pb$ ratios decreased markedly to reach 1.158 in the uppermost sediment level.

5. Discussion

5.1 Variations in sedimentary inputs and biogeochemical conditions

Prior to around 8000 BC, sedimentation rates, concentrations of terrigenous elements were high whereas TOC concentration were low (Fig.3). During this period (end of the Late Glacial Period), cold conditions favored erosion of bedrock probably by the small glacier in the watershed. During the Holocene climatic optimum, from the end of the Late Glacial Period (around 10,800 BC), TOC concentrations increased to reach a maximum around 2400 BC (Fig.3). Simultaneously, the C/N ratio increased from 9.5, a value which is in the range of that of phytoplankton and/or aquatic macrophyte, to 15, characteristic of land derived OM. In parallel, $\delta^{13}C$ values increased to -27.9 ± 1.3 ‰ (Fig. 3) which is also typical of terrestrial OM (Thevenon et al., 2012), thus the variations in TOC reflect a constant increase in inputs of soil derived OM. The higher temperatures during this period probably favored, the development of a soil and of vegetation as also described in other alpine lakes during the same period (Bajard et al., 2017, 2016; Mourier et al., 2010). This vegetation has stabilized the soils, thereby limiting erosion as shown by the low sedimentation rates and the low concentrations of minerogenic elements (Si, Al, Ti) (Fig. 3). From 2400 BC, the TOC decreased as also observed in other high Alpine Lakes (Giguet-Covex et al., 2011) and the C/N ratios tended toward those of phytoplankton and/or aquatic macrophytes. Concentrations of minerogenic elements increased in parallel indicating increased inputs of mineral matter. This corresponds to the onset of the Holocene Neoglacial period in which glaciers advanced in the Mont Blanc massif (Le Roy et al., 2015) and the Ecrins-Pelvoux massifs (Le Roy et al., 2017) in phase with a regional increase in mineral matter inputs and/or erosion, as recorded in Lake Bramant (Guyard et al., 2007), Lake Anterne (Giguet-Covex et al., 2011), Lake Petit (Brisset et al., 2013), Lake Bourget (Arnaud et al., 2012), Lake la Thuile (Bajard et al., 2016) and Lake Savine (Sabatier et al., 2017).

From the Iron Age on, sedimentation rates increased due to human activity, which according to (Arnaud et al., 2016) was responsible for general erosion at local scale in the Northern French Alps from this date on. Increasing pastoral activities in the catchment plus deforestation leaded to a continuous increase in the sedimentation rate until around AD 1340 when Black Death pandemic ravaged Europe. After a period of stagnation erosion resumed around AD 1500 and increased exponentially during the two last centuries. The most recent episode which is marked by both an increase in the sedimentation rates and in Ti or Al concentrations in the shallowest sediment levels (Fig. 3) is probably linked to human activities: industrialization of the valley and the building of roads and railways lines in the 19th century AD that probably increased the supply of atmospheric dust and of the ski resort in the Lake Robert watershed in the second half of the 20th century AD.

Other studies have evidenced fluctuations in lake water oxygenation in alpine lakes during the same period. Considering bottom water oxygenation, higher values of the Fe/Mn ratio at the end of the Late Glacial Period and Early Holocene (from prior to 10,800 BC to 8400 cal BC) and during the neoglacial period from around 2400 BC with a maximum in 500 BC, could reflect episodes of oxygen deficiency in lake bottom waters during the cold periods as also inferred in the neighboring Lake la Thuile (Bajard et al., 2016). However, the absence of a correlation between the Fe/Mn ratios and the TMM concentrations suggests that such redox changes have had no influence or only negligible influence on retention of the TMM studied here.

5.2 Local history of TMM pollution

Paleolithic-Mesolithic-Neolithic-Chalcolithic (Prior to 10,800-2800 BC)

During this period, PbEF indicated no enrichments and prior to 5000 BC, the Pb isotopes signature (Fig. 5) resembled that of moraine samples reported by (Garçon et al., 2012). At the end of the Mesolithic (from around 5000 BC), PbEF did not change but the $^{206}Pb/^{207}Pb$ isotope ratios decreased. This decrease, which was concomitant with a slight decrease in $PbAR_T$, reflects a change in the source of Pb inputs to the lake. The most likely explanation is an increase in the contribution of the atmospheric Pb source and a comparative decrease in the contribution of the source of lithogenic Pb linked to the erosion decline in the watershed at the onset of the Holocene climatic optimum due soil stabilization by vegetation (Bajard et al., 2016).

CuEF and $CuAR_T$ increased from 10,800 BC on, which is before the emergence of Cu metallurgy in Europe (Carozza, 2010) and reached a maximum around 2800 BC. The parallel increase in Cu(EF) and TOC (Fig. 6) suggests that Cu deposition in lake sediment was enhanced by the influx of OM into the lake during the Holocene climatic optimum. This is not surprising, given the strong affinity of Cu for complexation with organic ligands (Irving and Williams, 1953) which largely controls its biogeochemical cycling (Benedetti et al., 1996; Hering and Morel, 1988; Kinniburgh et al., 1999).

Mercury enrichment factors also increased slowly and Hg concentrations were strongly correlated with TOC (Fig. 6) emphasizing the fact that during this pristine warm climate period, the in-lake accumulation of Hg was mostly driven by soil erosion (Schütze et al., 2018). This is consistent with the strong affinity of Hg for TOC (Lindberg and Harriss, 1974; Skyllberg et al., 2000), and in particular for soil OM known as a great sink for atmospheric Hg through vegetation uptake (Andersson, 1979; Demers et al., 2013; Guédron et al., 2013). This suggests that both atmospherically derived Hg and dissolved organic carbon bound Hg that leached

from the watershed were likely scavenged onto the OM and/or recycled onto sulfidized OM during early diagenesis in the lake sediment (Feyte et al., 2012).

Bronze Age (2800 -1000 BC)

The first significant peak of PbEF occurred around 2080 BC while the maximum HgEF values between around 1800 and 1600 BC were 4 to 5 times higher than those observed between 4000 and 2000 BC (Fig. 4). SbEF values were also high around 1350 BC during the Bronze Age. As already mentioned, the study area has numerous metal ores. In the Bronze Age, chalcopyrite rich veins were exploited in the Rousses massif from 2200 BC until 1700 BC (Bailly-Maitre and Gonon, 2008; Carozza, 2010). These mines are located 15 km from Lake Robert as the crow flies. The occurrence of grey Cu containing Sb in the form of bournonite and tetrahedrite has already been reported in ores exploited in the Bronze Age (Chermette and Termier, 1970). Analysis of a chalcopyrite sample from the ores exploited in the Bronze Age had high (115 µg g^{-1}) Hg content. This ore was exploited by firesetting (Bailly-Maitre and Gonon, 2008) which probably favored the release of Hg and Sb into the atmosphere. Although CuEF generally decreased in the Bronze Age following the decline of primary production, the peak shoulders in the Cu distribution and especially in $CuAR_T$ observed around 1800 BC (Fig. 4), could also reflect mining pollution. The Pb isotopic composition could be interpreted as the reflection of two end-members: a natural background and that of Rio Tinto mines that were already exploited at that time (Leblanc et al., 2000), However, the Hg and Sb pollution and the similarity between the Pb isotopic ratios in lake sediments and those of the bournonite and the galena of the Cu-Pb-Ag vein samples from the Rousses Massif (Garçon et al., 2012) suggest that early Cu mining in the Rousses Massif was

responsible for most of the Pb, and of all the Hg and Sb pollution of Lake Robert during the Bronze Age. Only slight increases in HgAR have been reported in the high altitude alpine Lake Meidsee during the Bronze Age (Thevenon et al., 2011). Consequently, the marked rise in $HgAR_T$, which is the equivalent of that of the Industrial era (Fig. 4), likely results from rapid recycling of Hg emitted in the vicinity of this mining area.

Iron Age-Roman Empire (800 BC -AD 500 AD)

The main Pb pollution event occurred between ca 500 BC and AD 20 with a maximum in ca 320 BC (Iron Age). According to the Pb isotopic composition, the pollution did not originate from local ores. One possible provenance of the pollution is Sardinia (Baronia region) (Fig. 5).

Later, after AD 20 during the Roman Empire, although data are scarce, the EF Pb indicated low Pb pollution and the Pb composition reflected either local Pb or a mixture of natural and Iberian Pb. Archeological data plead for the second hypothesis. Indeed, there are no archeological proofs for an exploitation of the Bronze Age mines during the Roman Empire (Bailly-Maître, 2014).

After the major pollution event in the Bronze Age, EF and AR_T of Sb and Hg remained relatively low. In agreement with Pb isotope ratios, these results also plead for the abandonment of the Bronze Age mines in favor of distant mines during the Iron Age and the Roman Empire.

Medieval -Modern-Industrial periods (AD 800-1980)

During the medieval period, PbEF and $PbAR_T$ reached a peak around AD 1215. Broad peaks of $HgAR_T$, $SbAR_T$ and SbEF were also visible from 900 to AD 1340.

The Pb isotope signatures are consistent with pollution caused by exploitation of the local Brandes Ag-Pb mine in Rousses Massif that was intensely exploited at that time (Bailly-Maître, 1996; Chermette and Termier, 1970). High concentrations of Hg and Sb were measured in the galena found in the soils of a workshop (Hg=3.6 µg g^{-1}; Sb=1986 µg g^{-1}) and in the mine tailings (Hg=2.1 µg g^{-1}; Sb=1022 µg g^{-1}) (Table 2). Pollution declined after AD 1340 because the mine closed in AD 1330 due to climate cooling, the exhaustion of some ores but also due to the Black Death pandemic in Europe (Bailly-Maître, 1996).

After the medieval period, the isotopic Pb composition evolved from that of the local Pb ores in AD 1790 to that of French industrial Pb or of leaded gasoline in 1976 (Elbaz-Poulichet et al., 1986) (Fig. 4).

5.3 Deciphering local and regional mining contamination

This study highlights increased atmospheric TMM pollution in Lake Robert in prehistoric and historical times: the Bronze Age (2000-800 BC), the Iron Age and Roman Empire (800 BC- AD 500), the medieval period (AD 500-1500), the modern and industrial periods (AD 1500-present).

Pb pollution in the Bronze Age has been also reported in Spain (Martínez Cortizas et al., 2016) but in that case, pollution, which was generally low and was not recorded in all European archives was generally linked to small local exploitations. The Pb isotope ratios in Lake Robert reveal mixed sources in the form of local natural Pb from moraines and Pb from local minerals found in the Cu ores that were exploited at that time. The high level of Hg and Sb pollution observed in Lake Robert has not been observed in other regional archives (Mont Blanc ice, Etang de la Gruère mire). The source of pollution was thus probably only local and although the

AR_T increased by a factor of 7 (Hg) and 9 (Sb) compared to pre-Bronze Age values, the emissions were too small to affect distant locations.

Pb pollution is ubiquitous in the records of three other periods in southwestern or western Europe in the Swiss Jura (Shotyk et al., 1998), in Swiss Wallis (Thevenon et al., 2011), in a French Pyrenean mire (Hansson et al., 2017), in a northwestern Spanish mire (Martínez Cortizas et al., 2016-Fig. 7), in a coastal Mediterranean lagoon (Elbaz-Poulichet et al., 2011), in Atlantic shelf sediments (Mil-Homens et al., 2017) in Mont Blanc (Preunkert et al., 2019) and Greenland ice (Hong et al., 1994; McConnell et al., 2018- Fig. 7; Rosman et al., 1997). In the Iron Age and Roman Empire, this pollution has mostly been attributed to atmospheric transport from the Iberian Peninsula where the Rio Tinto and Murcia mines were intensely exploited by the Phoenicians, the Carthaginians and subsequently by the Romans. During the Roman period, between 50 BC and AD 500, it has been estimated that Iberian mines contributed 60% of European production, British mines 10%, the remainder originated from comparatively smaller mines in Sardinia, Italy, Gaul, the Carpathians and the Balkans (Rosman et al., 1997). During the Iron Age before 50 BC, the isotopic composition in Lake Robert ressembles that of Sardinian Pb (Baronia). Later during the Roman period, Pb isotope composition could reflect a mixture of local background Pb and Iberian Pb. Light Hg pollution was also detected in the Iron Age-Roman Empire in the archive studied here as well as in several archives in the Alps (Meidsee sediments Thevenon et al., 2011-Fig. 7), in the Jura (Etang de la Guère mire, Roos-Barraclough and Shotyk, 2003- Fig. 7), in the Black Forest (Glaswaldsee sediments, Schütze et al., 2018- Fig. 7), in Spain (Penido Vello mire, (Martinez-Cortizas et al., 1999). This pollution is generally attributed to the mining of the Almaden Hg ore (i.e., cinnabar) but local mining and/or metallurgy cannot be

excluded. Regarding Sb, observations in mires in southwestern Europe (Pyrenean, Hansson et al., 2017; Swiss Jura, (Shotyk et al., 1996) and in the Arctic (Krachler et al., 2008) and in Mont Blanc ice (Preunkert et al., 2019) also produced evidence for pollution in the Iron Age-Roman period that was attributed to mining in the Iberian Peninsula.

Pb pollution in the Middle Ages is also reported in all European and Arctic archives. At that time, many local Ag-Pb ores were exploited throughout Europe primarily to make coins. Pb isotope ratios in Lake Robert mainly reflect pollution caused by local mines. Hg pollution also occurred in the Middle Ages, but recent studies suggest that deforestation and burning of biomass could also have played an important role (Elbaz-Poulichet et al., 2011; Enrico et al., 2017).

In the modern period, Pb, Hg and Sb AR_T increased in Lake Robert to reach maximum values of 2723 µg m^{-2} yr^{-1} (Pb) and 56 µg m^{-2} yr^{-1} (Sb) in AD 1976, and 5.14 µg m^{-2} yr^{-1} (Hg) in AD 1997. These values are 90 (Pb), 5 (Hg) and 20 (Sb) times higher than those of the pre-Bronze Age epoch.

This increase reflects both local and global TMM emissions. At the end of the 20^{th} century, Pb emissions and fallout were dominated by leaded antiknock compounds in gasoline, the use of which was forbidden in 2000 in Europe. At global scale, most Hg atmospheric pollution originated from fossil-fuel fired power plants (Pirrone et al., 2010). In the vicinity of Lake Robert, several local/regional sources of Hg including coal mining and electrometallurgy were identified by Guédron et al., (2016) which could also contribute to the observed pollution. Increasing concentrations, enrichments and accumulation rates of Sb have been observed in mires in Europe (Shotyk et al., 2005, 2004), Alpine ice (Van de Velde et al., 1999) and in polar ice in the Canadian Arctic (Krachler et al., 2008, 2005) since the

industrial revolution, illustrating the dramatic increase in global emissions of atmospheric Sb linked to the numerous uses of Sb (flame retardant, brake pads, additive to plastic) and also the mining of sulfide ores. In Lake Robert, the increase in $SbAR_T$ could be also due to the construction of the ski resort in the watershed that increased the AR of the sediment by remobilizing sediments/soils polluted by past mining activity. Similar remobilization processes of past pollution has been reported for pesticides (Sabatier et al., 2014) or P content (Bajard et al., 2018) in other lakes in the French Alps.

6. Conclusion

This multiproxy study in Lake Robert in the French Alps enabled the reconstruction of the history and origins (local vs regional) of TMM pollution over the last 10,000 years.

The variations in TMM enabled identification of four periods of pollution: the Bronze Age (1800-1000 BC), the Early Iron age and Roman Empire (800BC- AD 500), the Middle Ages (AD 500-1500), the modern and the industrial period (AD1500-2000).

One striking feature is the notable Hg and Sb pollution in the Bronze Age linked to early Cu mining in the Rousses Massif. During that period the Hg flux resembled the flux today. The significant increase in pollution in recent (20^{th} century AD) samples particularly in the case of Sb, is partly related to the remobilization of polluted soil particles during the construction of the ski resorts.

This study confirmed the importance of atmospheric Pb pollution particularly

during the Iron Age-Roman Empire, with a potential source in Sardinia during the Iron Age and in Iberia during the Roman Empire.

Last but not least it also shows that climate-induced environmental changes in a high altitude lake catchment can strongly affect Cu deposition and to a lesser extent that of Hg. During the Holocene climatic optimum (3350-2100 BC), the warmer climate conditions were favorable for soil development and hence a vegetation cover leading to an influx of OM and correlatively a substantial increase in Cu and Hg flux to the lake due to their strong affinity for MO.

Acknowledgements

We thank the municipality of Chamrousse for coring authorization and Chamrousse ski resort for access to Lake Robert. ^{14}C analyses were acquired thanks to the CNRS-INSU ARTEMIS national radiocarbon AMS measurement program at the *Laboratoire de Mesure* ^{14}C (LMC14) of the CEA (French Atomic Energy Commission) Institute at Saclay. The authors thank the *Environnement, Dynamique et Territoires de Montagne* for the X-ray fluorescence analyses. We also greatly acknowledge G. Sarret for providing soil and tailing samples from the Brandes mine and F. Giraud and E. Janots, of the Mineralogical Collection of the Grenoble Observatory of Earth Sciences (OSUG) for providing Chalcopyrite (N°255) samples. Thank also to R. Buscail, CEFREM Perpignan for providing the N data.

Data availability

Supplementary Information (SI) and datasets related to this article can be found at: Elbaz-Poulichet, Guedron, Develle, Freydier, Perrot, Rossi, Piot, Delpoux, Sabatier, (2019), “Lake Robert data Elbaz-Poulichet et al., 2019 QSR”, Mendeley Data, v1

http://dx.doi.org/10.17632/sswzys96rd.1

lab_ID	Depth (mm)	Age (BP)	Calibrated age ranges at 95% (cal BP)
SacA42475	120	320 ± 30	305 - 465
Poz-77372	180	830 ± 30	687 - 789
SacA42476	250	1150 ± 30	978 - 1170
Poz-77373	338	1920 ± 35	1740 - 1948
SacA42477	390	2660 ± 30	2742 - 2844
SacA42478	470	3595 ± 30	3836 - 3976
SacA42479	550	4900 ± 30*	5588 – 5707*
Poz-77374	630	6040 ± 40	6786 - 6995
SacA42480	690	8200 ± 45	9024 - 9286

Table 1: ^{14}C dates for Lake Robert (ROB15-P5). * rejected date.

Sample ID	Ore type	Location	Cu (µg/g)	Sb (µg/g)	THg (µg/g)	Pb (µg/g)
LBV1	Bournonite ($PbCuSbS_3$)	Lake Blanc Huez	N.A.	N.A.	202	N.A.
LBV2	Malachite ($Cu_2CO_3(OH)_2$)	Lake Blanc Huez	N.A.	N.A.	30	N.A.
LBV3	Galena (PbS)	Lake Blanc Huez	N.A.	N.A.	2.4	N.A.
LBV7	Barite ($BaSO_4$)	Lake Blanc Huez	N.A.	N.A.	0.44	N.A.
Halde Soil	-	Brandes Mine	5311	1986	3.6	17224
Halde tailing	-	Brandes Mine	1545	1022	2.1	26351
Halde Galena	Galena (PbS)	Brandes Mine	232	691	N.A.	41046
OSUG-00248	Chalcopyrite	Demoiselles Mine	N.A.	N.A.	112	N.A.

Table 2 : Cu, Sb, Hg and Pb elemental content of minerals and mining soils or taillings of the Grandes Rousses massif. Samples LBV1, LBV2, LBV3 and LBV7 are from the Lake Blanc Huez (N 45° 6' 52", E 6° 6' 21") with their Pb isotopic composition published in (Garçon et al., 2012), soil, mine tailing and Galena from the Brandes mine (Huez, N 45° 5' 7.2", E 6° 5' 6.5") where provided by G. Sarret and chalcopyrite of the Demoiselles mine (Vaujany, N 45°10' 44", E 6° 7' 52" , reference OSUG-00248) was provided by the Mineralogical Collection of the Grenoble Observatory of Earth Sciences (OSUG).

References

Achterberg, E.P., Van Den Berg, C.M.G., Boussemart, M., Davison, W., 1997. Speciation and cycling of trace metals in Esthwaite Water: a productive English lake with seasonal deep-water anoxia. Geochim. Cosmochim. Acta 61, 5233–5253.

Alfonso, S., Grousset, F., Massé, L., Tastet, J.-P., 2001. A European lead isotope signal recorded from 6000 to 300 years BP in coastal marshes (SW France). Atmos. Environ. 35, 3595–3605.

Andersson, A., 1979. Mercury in soils, in the Biogeochemistry of mercury in the environment, edited by JO Nriagu, 79-112.

Arnaud, F., Poulenard, J., Giguet-Covex, C., Wilhelm, B., Révillon, S., Jenny, J.-P., Revel, M., Enters, D., Bajard, M., Fouinat, L., 2016. Erosion under climate and human pressures: An alpine lake sediment perspective. Quat. Sci. Rev. 152, 1–18.

Arnaud, F., Révillon, S., Debret, M., Revel, M., Chapron, E., Jacob, J., Giguet-Covex, C., Poulenard, J., Magny, M., 2012. Lake Bourget regional erosion patterns reconstruction reveals Holocene NW European Alps soil evolution and paleohydrology. Quat. Sci. Rev. 51, 81–92.

Artioli, G., Angelini, I., Tecchiati, U., Pedrotti, A., 2015. Eneolithic copper smelting slags in the Eastern Alps: Local patterns of metallurgical exploitation in the Copper Age. J. Archaeol. Sci. 63, 78–83.

Bailly-Maître, M.-C., 1996. Brandes-en-Oisans: incidences d'un milieu alpin sur une exploitation minière médiévale. Actes des congrès la Société d'archéologie médiévale 5, 235–245.

Bailly-Maître, M.-C., 2014. De l'or, de l'argent, du cuivre, du plomb, du fer, du cobalt, de l'anthracite et des quartz hyalins. Quatre mille ans d'histoire minière en Oisans. Collect. EDYTEM. Cah. géographie 17, 41–52.

Bailly-Maitre, M.-C., Gonon, T., 2008. L'exploitation de la chalcopyrite à l'âge du Bronze dans le massif des Rousses en Oisans (Isère): premiers éléments. Editions du CTHS.

Bajard, M., Etienne, D., Quinsac, S., Dambrine, E., Sabatier, P., Frossard, V., Gaillard, J., Develle, A.-L., Poulenard, J., Arnaud, F., 2018. Legacy of early anthropogenic effects on recent lake eutrophication (Lake Bénit, northern French Alps). Anthropocene 24, 72–87.

Bajard, M., Poulenard, J., Sabatier, P., Etienne, D., Ficetola, F., Chen, W., Gielly, L., Taberlet, P., Develle, A.-L., Rey, P.-J., 2017. Long-term changes in alpine pedogenetic processes: Effect of millennial agro-pastoralism activities (French-Italian Alps). Geoderma 306, 217–236.

Bajard, M., Sabatier, P., David, F., Develle, A.-L., Reyss, J.-L., Fanget, B., Malet, E., Arnaud, D., Augustin, L., Crouzet, C., 2016. Erosion record in Lake La Thuile sediments (Prealps, France): Evidence of montane landscape dynamics throughout the Holocene. The Holocene 26, 350–364.

Balslev-Clausen, D., Dahl, T.W., Saad, N., Rosing, M.T., 2013. Precise and accurate δ 13 C analysis of rock samples using Flash Combustion–Cavity Ring Down Laser Spectroscopy. J. Anal. At. Spectrom. 28, 516–523.

Belzile, N., Chen, Y.-W., Wang, Z., 2001. Oxidation of antimony (III) by amorphous iron and manganese oxyhydroxides. Chem. Geol. 174, 379–387.

Benedetti, M.F., Van Riemsdijk, W.H., Koopal, L.K., Kinniburgh, D.G., Gooddy, D.C., Milne, C.J., 1996. Metal ion binding by natural organic matter: from the model to

the field. Geochim. Cosmochim. Acta 60, 2503–2513.

Bindler, R., Renberg, I., Rydberg, J., Andrén, T., 2009. Widespread waterborne pollution in central Swedish lakes and the Baltic Sea from pre-industrial mining and metallurgy. Environ. Pollut. 157, 2132–2141.

Bindler, R., Rydberg, J., Renberg, I., 2011. Establishing natural sediment reference conditions for metals and the legacy of long-range and local pollution on lakes in Europe. J. Paleolimnol. 45, 519–531.

Blaauw, M., 2010. Methods and code for 'classical'age-modelling of radiocarbon sequences. Quat. Geochronol. 5, 512–518.

Bourgarit, D., Rostan, P., Burger, E., Carozza, L., Mille, B., Artioli, G., 2008. The beginning of copper mass production in the western Alps: the Saint-Véran mining area reconsidered. Hist. Metall. 42, 1–11.

Brännvall, M.-L., Bindler, R., Emteryd, O., Nilsson, M., Renberg, I., 1997. Stable isotope and concentration records of atmospheric lead pollution in peat and lake sediments in Sweden. Water. Air. Soil Pollut. 100, 243–252.

Brännvall, M.-L., Bindler, R., Renberg, I., Emteryd, O., Bartnicki, J., Billström, K., 1999. The Medieval metal industry was the cradle of modern large-scale atmospheric lead pollution in northern Europe. Environ. Sci. Technol. 33, 4391–4395.

Brisset, E., Miramont, C., Guiter, F., Anthony, E.J., Tachikawa, K., Poulenard, J., Arnaud, F., Delhon, C., Meunier, J.-D., Bard, E., 2013. Non-reversible geosystem destabilisation at 4200 cal. BP: Sedimentological, geochemical and botanical markers of soil erosion recorded in a Mediterranean alpine lake. The Holocene 23, 1863–1874.

Brüchmann, C., Negendank, J.F.W., 2004. Indication of climatically induced natural

eutrophication during the early Holocene period, based on annually laminated sediment from Lake Holzmaar, Germany. Quat. Int. 123, 117–134.

Carignan, J., Hild, P., Mevelle, G., Morel, J., Yeghicheyan, D., 2001. Routine analyses of trace elements in geological samples using flow injection and low pressure on□line liquid chromatography coupled to ICP□MS: a study of geochemical reference materials BR, DR□N, UB□N, AN□G and GH. Geostand. Geoanalytical Res. 25, 187–198.

Carozza, L., 2010. Glacial Fluctuations and Exploitation of Copper Resources, in: In: Mining in European History and Its Impact on Environment and Human Societies, Prooceedings of the 1st Mining in European History- Conference of the SFB-HIMAT, 12-15 Novembrer 2009, Innsbruck. pp. 81–90.

Chapron, E., Faïn, X., Magand, O., Charlet, L., Debret, M., Mélières, M.A., 2007. Reconstructing recent environmental changes from proglacial lake sediments in the Western Alps (Lake Blanc Huez, 2543 m asl, Grandes Rousses Massif, France). Palaeogeogr. Palaeoclimatol. Palaeoecol. 252, 586–600.

Chen, Y.-W., Deng, T.-L., Filella, M., Belzile, N., 2003. Distribution and early diagenesis of antimony species in sediments and porewaters of freshwater lakes. Environ. Sci. Technol. 37, 1163–1168.

Chermette, A., Termier, P., 1970. Minéralogie : Sur les anciennes mines de l'Oisans. Publ. la Société Linnéenne Lyon 21–30.

Clavel, M., 1963. Contribution à l'étude métallogénique de la région d'Allemont (Massif de Belledonne-Isère)-Alpes françaises.

Cooke, C.A., Balcom, P.H., Kerfoot, C., Abbott, M.B., Wolfe, A.P., 2011. Pre-Colombian mercury pollution associated with the smelting of argentiferous ores in the Bolivian Andes. AMBIO A J. Hum. Environ. 40, 18–25.

Cooke, C.A., Bindler, R., 2015. Lake sediment records of preindustrial metal pollution, in: Environmental Contaminants. Springer, pp. 101–119.

Davison, W., 1993. Iron and manganese in lakes. Earth-Science Rev. 34, 119–163.

De Vleeschouwer, F., Fagel, N., Cheburkin, A., Pazdur, A., Sikorski, J., Mattielli, N., Renson, V., Fialkiewicz, B., Piotrowska, N., Le Roux, G., 2009. Anthropogenic impacts in North Poland over the last 1300 years—a record of Pb, Zn, Cu, Ni and S in an ombrotrophic peat bog. Sci. Total Environ. 407, 5674–5684.

Demers, J.D., Blum, J.D., Zak, D.R., 2013. Mercury isotopes in a forested ecosystem: Implications for air□surface exchange dynamics and the global mercury cycle. Global Biogeochem. Cycles 27, 222–238.

Elbaz-Poulichet, F., Dezileau, L., Freydier, R., Cossa, D., Sabatier, P., 2011. A 3500-year record of Hg and Pb contamination in a mediterranean sedimentary archive (The Pierre Blanche Lagoon, France). Environ. Sci. Technol. 45.

Elbaz-Poulichet, F., Holliger, P., Martin, J.M., Petit, D., 1986. Stable lead isotopes ratios in major french rivers and estuaries. Sci. Total Environ. 54.

Elbaz-Poulichet, F., Holliger, P., Wen Huang, W., Martin, J.-M., 1984. Lead cycling in estuaries, illustrated by the Gironde estuary, France. Nature 308.

Enrico, M., Le Roux, G., Heimbürger, L.-E., Van Beek, P., Souhaut, M., Chmeleff, J., Sonke, J.E., 2017. Holocene atmospheric mercury levels reconstructed from peat bog mercury stable isotopes. Environ. Sci. Technol. 51, 5899–5906.

Feyte, S., Gobeil, C., Tessier, A., Cossa, D., 2012. Mercury dynamics in lake sediments. Geochim. Cosmochim. Acta 82, 92–112.

Gallon, C., Tessier, A., Gobeil, C., Alfaro-De La Torre, M.C., 2004. Modeling diagenesis of lead in sediments of a Canadian Shield lake. Geochim. Cosmochim. Acta 68, 3531–3545.

García-Alix, A., Jimenez-Espejo, F.J., Lozano, J.A., Jiménez-Moreno, G., Martinez-Ruiz, F., Sanjuán, L.G., Jiménez, G.A., Alfonso, E.G., Ruiz-Puertas, G., Anderson, R.S., 2013. Anthropogenic impact and lead pollution throughout the Holocene in Southern Iberia. Sci. Total Environ. 449, 451–460.

Garçon, M., Chauvel, C., Chapron, E., Faïn, X., Lin, M., Campillo, S., Bureau, S., Desmet, M., Bailly-Maître, M.-C., Charlet, L., 2012. Silver and lead in high-altitude lake sediments: Proxies for climate changes and human activities. Appl. Geochemistry 27, 760–773.

Giguet-Covex, C., Arnaud, F., Poulenard, J., Disnar, J.-R., Delhon, C., Francus, P., David, F., Enters, D., Rey, P.-J., Delannoy, J.-J., 2011. Changes in erosion patterns during the Holocene in a currently treeless subalpine catchment inferred from lake sediment geochemistry (Lake Anterne, 2063 m asl, NW French Alps): the role of climate and human activities. The Holocene 21, 651–665.

Guédron, S., Amouroux, D., Sabatier, P., Desplanque, C., Develle, A.-L., Barre, J., Feng, C., Guiter, F., Arnaud, F., Reyss, J.L., 2016. A hundred year record of industrial and urban development in French Alps combining Hg accumulation rates and isotope composition in sediment archives from Lake Luitel. Chem. Geol. 431, 10–19.

Guédron, S., Grangeon, S., Jouravel, G., Charlet, L., Sarret, G., 2013. Atmospheric mercury incorporation in soils of an area impacted by a chlor-alkali plant (Grenoble, France): contribution of canopy uptake. Sci. Total Environ. 445, 356–364.

Guedron, S., Grangeon, S., Lanson, B., Grimaldi, M., 2009. Mercury speciation in a tropical soil association; Consequence of gold mining on Hg distribution in French Guiana. Geoderma 153, 331–346.

Guédron, S., Tolu, J., Brisset, E., Sabatier, P., Perrot, V., Bouchet, S., Develle, A.L., Bindler, R., Cossa, D., Fritz, S.C., 2019. Late Holocene volcanic and anthropogenic mercury deposition in the western Central Andes (Lake Chungará, Chile). Sci. Total Environ. 662, 903–914.

Guyard, H., Chapron, E., St-Onge, G., Anselmetti, F.S., Arnaud, F., Magand, O., Francus, P., Mélières, M.-A., 2007. High-altitude varve records of abrupt environmental changes and mining activity over the last 4000 years in the Western French Alps (Lake Bramant, Grandes Rousses Massif). Quat. Sci. Rev. 26, 2644–2660.

Hansson, S. V, Claustres, A., Probst, A., De Vleeschouwer, F., Baron, S., Galop, D., Mazier, F., Le Roux, G., 2017. Atmospheric and terrigenous metal accumulation over 3000 years in a French mountain catchment: Local vs distal influences. Anthropocene 19, 45–54.

Hering, J.G., Morel, F.M.M., 1988. Humic acid complexation of calcium and copper. Environ. Sci. Technol. 22, 1234–1237.

Hong, S., Candelone, J.-P., Patterson, C.C., Boutron, C.F., 1994. Greenland ice evidence of hemispheric lead pollution two millennia ago by Greek and Roman civilizations. Science (80-.). 265, 1841–1843.

Höppner, B., Bartelheim, M., Huijsmans, M., Krauss, R., MARTINEK, K., Pernicka, E., Schwab, R., 2005. Prehistoric copper production in the Inn Valley (Austria), and the earliest copper in central Europe. Archaeometry 47, 293–315.

Irving, H., Williams, Rjp., 1953. 637. The stability of transition-metal complexes. J. Chem. Soc. 3192–3210.

Kinniburgh, D.G., van Riemsdijk, W.H., Koopal, L.K., Borkovec, M., Benedetti, M.F., Avena, M.J., 1999. Ion binding to natural organic matter: competition,

heterogeneity, stoichiometry and thermodynamic consistency. Colloids Surfaces A Physicochem. Eng. Asp. 151, 147–166.

Koinig, K.A., Shotyk, W., Lotter, A.F., Ohlendorf, C., Sturm, M., 2003. 9000 years of geochemical evolution of lithogenic major and trace elements in the sediment of an alpine lake–the role of climate, vegetation, and land-use history. J. Paleolimnol. 30, 307–320.

Krachler, M., Zheng, J., Fisher, D., Shotyk, W., 2008. Atmospheric Sb in the Arctic during the past 16,000 years: Responses to climate change and human impacts. Global Biogeochem. Cycles 22.

Krachler, M., Zheng, J., Koerner, R., Zdanowicz, C., Fisher, D., Shotyk, W., 2005. Increasing atmospheric antimony contamination in the northern hemisphere: snow and ice evidence from Devon Island, Arctic Canada. J. Environ. Monit. 7, 1169–1176.

Küttner, A., Mighall, T.M., De Vleeschouwer, F., Mauquoy, D., Cortizas, A.M., Foster, I.D.L., Krupp, E., 2014. A 3300-year atmospheric metal contamination record from Raeburn Flow raised bog, south west Scotland. J. Archaeol. Sci. 44, 1–11.

Kylander, M.E., Weiss, D.J., Cortizas, A.M., Spiro, B., Garcia-Sanchez, R., Coles, B.J., 2005. Refining the pre-industrial atmospheric Pb isotope evolution curve in Europe using an 8000 year old peat core from NW Spain. Earth Planet. Sci. Lett. 240, 467–485.

Lacroix, A., 1893. 1913-Minéralogie de la France et de ses colonies. Paris, Libr. Polytech. Béranger 5.

Le Roy, M., Deline, P., Carcaillet, J., Schimmelpfennig, I., Ermini, M., Team, A., 2017. 10Be exposure dating of the timing of Neoglacial glacier advances in the Ecrins-Pelvoux massif, southern French Alps. Quat. Sci. Rev. 178, 118–138.

Le Roy, M., Nicolussi, K., Deline, P., Astrade, L., Edouard, J.-L., Miramont, C., Arnaud, F., 2015. Calendar-dated glacier variations in the western European Alps during the Neoglacial: the Mer de Glace record, Mont Blanc massif. Quat. Sci. Rev. 108, 1–22.

Leblanc, M., Morales, J.A., Borrego, J., Elbaz-Poulichet, F., 2000. 4,500-year-old mining pollution in southwestern Spain: Long-term implications for modern mining pollution. Econ. Geol. 95.

Lee, C.S.L., Qi, S., Zhang, G., Luo, C., Zhao, L.Y.L., Li, X., 2008. Seven thousand years of records on the mining and utilization of metals from lake sediments in central China. Environ. Sci. Technol. 42, 4732–4738.

Lindberg, S.E., Harriss, R.C., 1974. Mercury-organic matter associations in estuarine sediments and interstitial water. Environ. Sci. Technol. 8, 459–462.

Loizeau, J.-L., Span, D., Coppee, V., Dominik, J., 2001. Evolution of the trophic state of Lake Annecy (eastern France) since the last glaciation as indicated by iron, manganese and phosphorus speciation. J. Paleolimnol. 25, 205–214.

Manteca, J.-I., Ros-Sala, M., Ramallo-Asensio, S., Navarro-Hervás, F., Rodríguez-Estrella, T., Cerezo-Andreo, F., Ortiz-Menéndez, J.-E., de-Torres, T., Martínez-Andreu, M., 2017. Early metal pollution in southwestern Europe: the former littoral lagoon of El Almarjal (Cartagena mining district, SE Spain). A sedimentary archive more than 8000 years old. Environ. Sci. Pollut. Res. 24, 10584–10603.

Martinez-Cortizas, A., Pontevedra-Pombal, X., Garcia-Rodeja, E., Novoa-Munoz, J.C., Shotyk, W., 1999. Mercury in a Spanish peat bog: Archive of climate change and atmospheric metal deposition. Science (80-.). 284, 939.

Martinez-Cortizas, A., Pontevedra-Pombal, X., Munoz, J.C.N., García-Rodeja, E.,

1997. Four thousand years of atmospheric Pb, Cd and Zn deposition recorded by the ombrotrophic peat bog of Penido Vello (Northwestern Spain). Water. Air. Soil Pollut. 100, 387–403.

Martínez Cortizas, A., López-Merino, L., Bindler, R., Mighall, T., Kylander, M.E., 2016. Early atmospheric metal pollution provides evidence for Chalcolithic/Bronze Age mining and metallurgy in Southwestern Europe. Sci. Total Environ. 545–546, 398–406.

McConnell, J.R., Wilson, A.I., Stohl, A., Arienzo, M.M., Chellman, N.J., Eckhardt, S., Thompson, E.M., Pollard, A.M., Steffensen, J.P., 2018. Lead pollution recorded in Greenland ice indicates European emissions tracked plagues, wars, and imperial expansion during antiquity. Proc. Natl. Acad. Sci. 115, 5726–5731.

Meyers, P.A., Teranes, J.L., 2001. Tracking Environmental Change Using Lake Sediments, eds Last WM, Smol JP.

Mil-Homens, M., Vale, C., Brito, P., Naughton, F., Drago, T., Raimundo, J., Anes, B., Schmidt, S., Caetano, M., 2017. Insights of Pb isotopic signature into the historical evolution and sources of Pb contamination in a sediment core of the southwestern Iberian Atlantic shelf. Sci. Total Environ. 586, 473–484.

Monna, F., Camizuli, E., Revelli, P., Biville, C., Thomas, C., Losno, R., Scheifler, R., Bruguier, O., Baron, S., Chateau, C., 2011. Wild brown trout affected by historical mining in the Cévennes National Park, France. Environ. Sci. Technol. 45, 6823–6830.

Monna, F., Galop, D., Carozza, L., Tual, M., Beyrie, A., Marembert, F., Chateau, C., Dominik, J., Grousset, F.E., 2004. Environmental impact of early Basque mining and smelting recorded in a high ash minerogenic peat deposit. Sci. Total Environ. 327, 197–214.

Moulin, B., Thirault, E., Vital, J., Bailly-Maître, M.-C., 2010. Quatre années de prospection sur les extractions de cuivre de l'âge du Bronze ancien dans le massif des Rousses en Oisans (Isère et Savoie, France), in: Dynamismes et Rythmes Évolutifs Des Sociétés de La Préhistoire Récente. Actualité de La Recherche. Actes Des 9e Rencontres Méridionales de Préhistoire Récente Saint-Georges-de-Didonne (17), 8 & 9 Octobre 2010. Archives d'écologie Préhistorique, pp. 341–369.

Mourier, B., Poulenard, J., Carcaillet, C., Williamson, D., 2010. Soil evolution and subalpine ecosystem changes in the French Alps inferred from geochemical analysis of lacustrine sediments. J. Paleolimnol. 44, 571–587.

Murozumi, M., Chow, T.J., Patterson, C., 1969. Chemical concentrations of pollutant lead aerosols, terrestrial dusts and sea salts in Greenland and Antarctic snow strata. Geochim. Cosmochim. Acta 33, 1247–1294.

Naeher, S., Gilli, A., North, R.P., Hamann, Y., Schubert, C.J., 2013. Tracing bottom water oxygenation with sedimentary Mn/Fe ratios in Lake Zurich, Switzerland. Chem. Geol. 352, 125–133.

Pacyna, J.M., 1987. Atmospheric Emissions of Arsenic, Cadmium, Lead and Mercuryfrom High Temperature Processes in Power Generation and Industry. Lead, Mercur. Cadmium Arsen. Environ. (eds. TC Hutchinson KM Meema). John Wiley Sons Ltd, USA 69–87.

Paul, D., Skrzypek, G., Fórizs, I., 2007. Normalization of measured stable isotopic compositions to isotope reference scales–a review. Rapid Commun. Mass Spectrom. An Int. J. Devoted to Rapid Dissem. Up□to□the□Minute Res. Mass Spectrom. 21, 3006–3014.

Pirrone, N., Cinnirella, S., Feng, X., Finkelman, R.B., Friedli, H.R., Leaner, J., Mason,

R., Mukherjee, A.B., Stracher, G.B., Streets, D.G., 2010. Global mercury emissions to the atmosphere from anthropogenic and natural sources. Atmos. Chem. Phys. 10, 5951–5964.

Pirrone, N., Mason, R., 2009. Mercury fate and transport in the global atmosphere. Dordrecht, Netherlands Springer. DOI 10, 970–978.

Pontevedra-Pombal, X., Mighall, T.M., Nóvoa-Muñoz, J.C., Peiteado-Varela, E., Rodríguez-Racedo, J., García-Rodeja, E., Martínez-Cortizas, A., 2013. Five thousand years of atmospheric Ni, Zn, As, and Cd deposition recorded in bogs from NW Iberia: prehistoric and historic anthropogenic contributions. J. Archaeol. Sci. 40, 764–777.

Preunkert, S., McConnell, J.R., Hoffmann, H., Legrand, M., Wilson, A.I., Eckhardt, S., Stohl, A., Chellman, N.J., Arienzo, M.M., Friedrich, R., 2019. Lead and antimony in basal ice from Col du Dome (French Alps) dated with radiocarbon: A record of pollution during antiquity. Geophys. Res. Lett.

Reimer, P.J., Bard, E., Bayliss, A., Beck, J.W., Blackwell, P.G., Ramsey, C.B., Buck, C.E., Cheng, H., Edwards, R.L., Friedrich, M., 2013. IntCal13 and Marine13 radiocarbon age calibration curves 0–50,000 years cal BP. Radiocarbon 55, 1869–1887.

Renberg, I., Brännvall, M.-L., Bindler, R., Emteryd, O., 2002. Stable lead isotopes and lake sediments—a useful combination for the study of atmospheric lead pollution history. Sci. Total Environ. 292, 45–54.

Renberg, I., Persson, M.W., Emteryd, O., 1994. Pre-industrial atmospheric lead contamination detected in Swedish lake sediments. Nature 368, 323.

Roos-Barraclough, F., Martinez-Cortizas, A., García-Rodeja, E., Shotyk, W., 2002. A 14 500 year record of the accumulation of atmospheric mercury in peat: volcanic

signals, anthropogenic influences and a correlation to bromine accumulation. Earth Planet. Sci. Lett. 202, 435–451.

Roos-Barraclough, F., Shotyk, W., 2003. Millennial-scale records of atmospheric mercury deposition obtained from ombrotrophic and minerotrophic peatlands in the Swiss Jura Mountains. Environ. Sci. Technol. 37, 235–244.

Rosman, K.J.R., Chisholm, W., Hong, S., Candelone, J.-P., Boutron, C.F., 1997. Lead from Carthaginian and Roman Spanish Mines Isotopically Identified in Greenland Ice Dated from 600 B.C. to 300 A.D.†. Environ. Sci. Technol. 31, 3413–3416.

Rydberg, J., Gälman, V., Renberg, I., Bindler, R., Lambertsson, L., Martínez-Cortizas, A., 2008. Assessing the stability of mercury and methylmercury in a varved lake sediment deposit. Environ. Sci. Technol. 42, 4391–4396.

Sabatier, P., Poulenard, J., Fanget, B., Reyss, J.-L., Develle, A.-L., Wilhelm, B., Ployon, E., Pignol, C., Naffrechoux, E., Dorioz, J.-M., 2014. Long-term relationships among pesticide applications, mobility, and soil erosion in a vineyard watershed. Proc. Natl. Acad. Sci. 111, 15647–15652.

Sabatier, P., Wilhelm, B., Ficetola, G.F., Moiroux, F., Poulenard, J., Develle, A.-L., Bichet, A., Chen, W., Pignol, C., Reyss, J.-L., 2017. 6-kyr record of flood frequency and intensity in the western Mediterranean Alps–Interplay of solar and temperature forcing. Quat. Sci. Rev. 170, 121–135.

Schütze, M., Tserendorj, G., Pérez-Rodríguez, M., Rösch, M., Biester, H., 2018. Prediction of Holocene Mercury Accumulation Trends by Combining Palynological and Geochemical Records of Lake Sediments (Black Forest, Germany). Geosciences 8, 358.

Serrano, O., Mateo, M.A., Dueñas-Bohórquez, A., Renom, P., López-Sáez, J.A.,

Cortizas, A.M., 2011. The Posidonia oceanica marine sedimentary record: a Holocene archive of heavy metal pollution. Sci. Total Environ. 409, 4831–4840.

Shotyk, W., Cheburkin, A.K., Appleby, P.G., Fankhauser, A., Kramers, J.D., 1996. Two thousand years of atmospheric arsenic, antimony, and lead deposition recorded in an ombrotrophic peat bog profile, Jura Mountains, Switzerland. Earth Planet. Sci. Lett. 145, E1–E7.

Shotyk, W., Chen, B., Krachler, M., 2005. Lithogenic, oceanic and anthropogenic sources of atmospheric Sb to a maritime blanket bog, Myrarnar, Faroe Islands. J. Environ. Monit. 7, 1148–1154.

Shotyk, W., Krachler, M., Chen, B., 2004. Antimony in recent, ombrotrophic peat from Switzerland and Scotland: Comparison with natural background values (5,320 to 8,020 14C yr BP) and implications for the global atmospheric Sb cycle. Global Biogeochem. Cycles 18.

Shotyk, W., Weiss, D., Appleby, P.G., Cheburkin, A.K., Frei, R., Gloor, M., Kramers, J.D., Reese, S., Van Der Knaap, W.O., 1998. History of atmospheric lead deposition since 12,370 14C yr BP from a peat bog, Jura Mountains, Switzerland. Science (80-.). 281, 1635–1640.

Skyllberg, U., Xia, K., Bloom, P.R., Nater, E.A., Bleam, W.F., 2000. Binding of mercury (II) to reduced sulfur in soil organic matter along upland-peat soil transects. J. Environ. Qual. 29, 855–865.

Stos-Gale, Z.A., Gale, N.H., 2009. Metal provenancing using isotopes and the Oxford archaeological lead isotope database (OXALID). Archaeol. Anthropol. Sci. 1, 195–213.

Sturges, W.T., Barrie, L.A., 1987. Lead 206/207 isotope ratios in the atmosphere of North America as tracers of US and Canadian emissions. Nature 329, 144.

Thevenon, F., Adatte, T., Spangenberg, J.E., Anselmetti, F.S., 2012. Elemental (C/N ratios) and isotopic (δ15Norg, δ13Corg) compositions of sedimentary organic matter from a high-altitude mountain lake (Meidsee, 2661 m asl, Switzerland): Implications for Lateglacial and Holocene Alpine landscape evolution. The Holocene 22, 1135–1142.

Thevenon, F., Guédron, S., Chiaradia, M., Loizeau, J.-L., Poté, J., 2011. (Pre-) historic changes in natural and anthropogenic heavy metals deposition inferred from two contrasting Swiss Alpine lakes. Quat. Sci. Rev. 30, 224–233.

Van de Velde, K., Ferrari, C., Barbante, C., Moret, I., Bellomi, T., Hong, S., Boutron, C., 1999. A 200 year record of atmospheric cobalt, chromium, molybdenum, and antimony in high altitude alpine firn and ice. Environ. Sci. Technol. 33, 3495–3501.

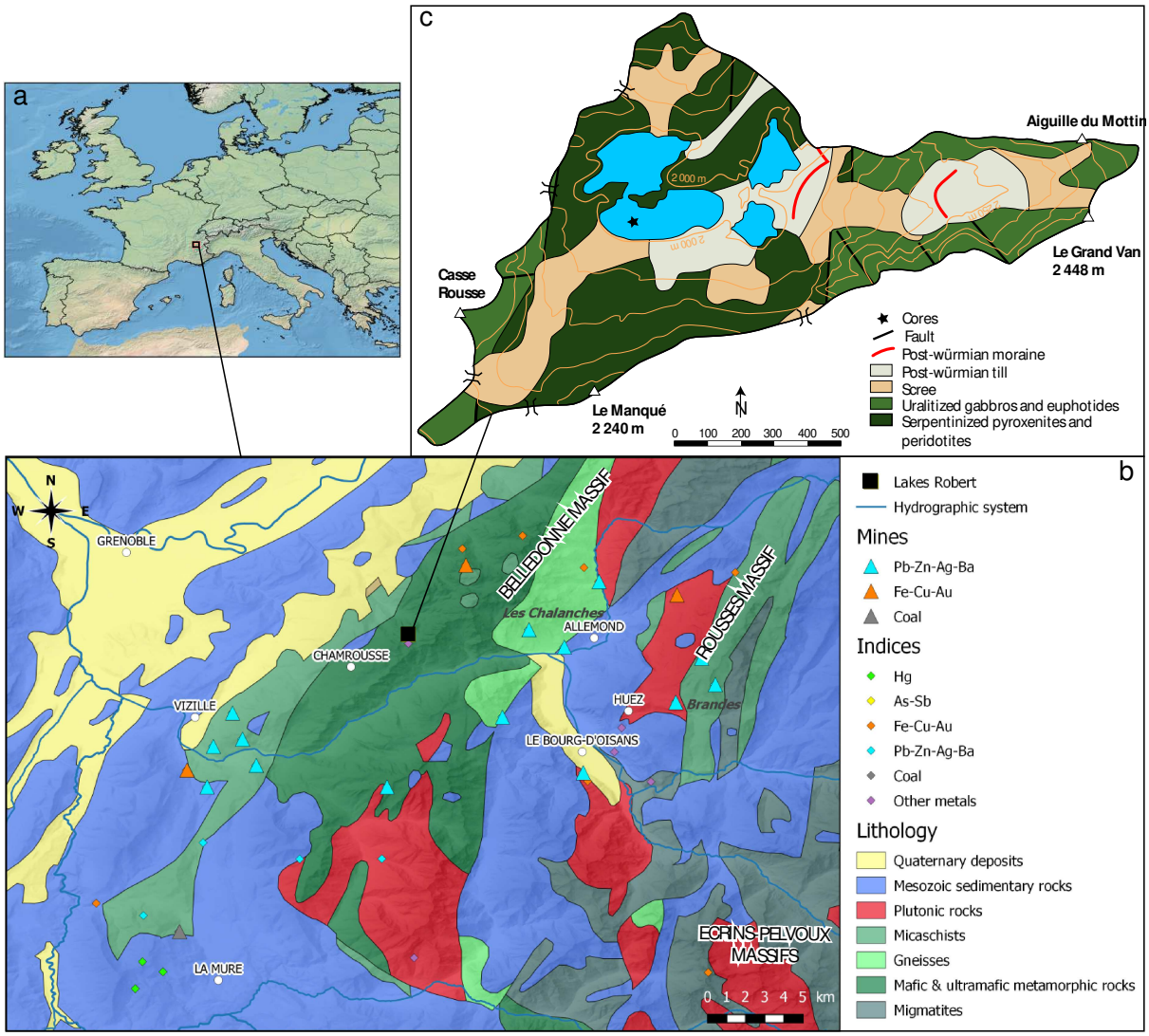

Fig. 1: Map showing the location of Lake Robert in the French Alps (a). Main geological units, the locations of recognized metal and metalloid indices and the locations of the main mining sites are shown in (b). The location of the coring site and the main lithological units of its drainage basin are shown in (c).

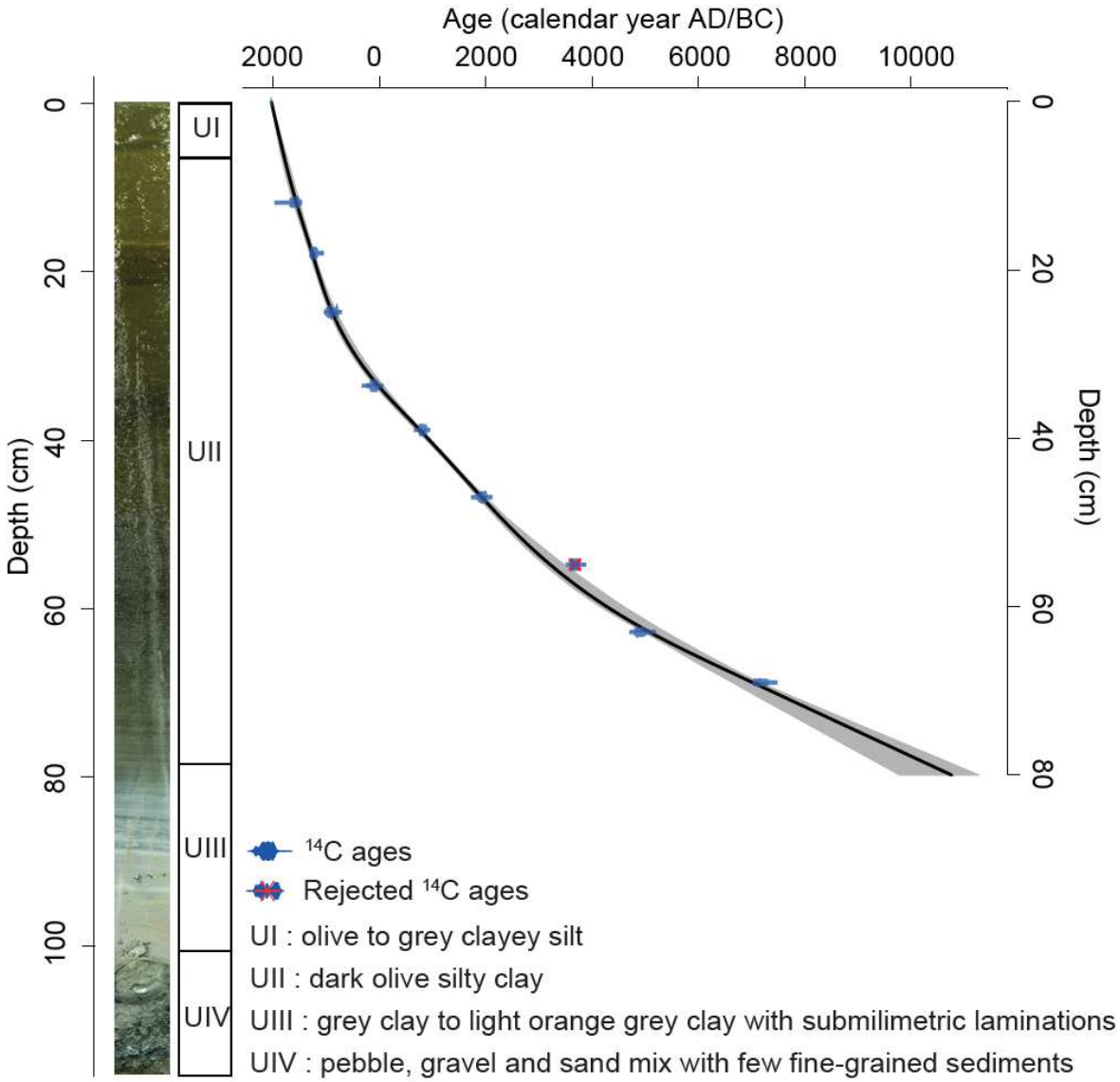

Fig. 2: Age-depth model and lithostratigraphic description of core ROB15-P5

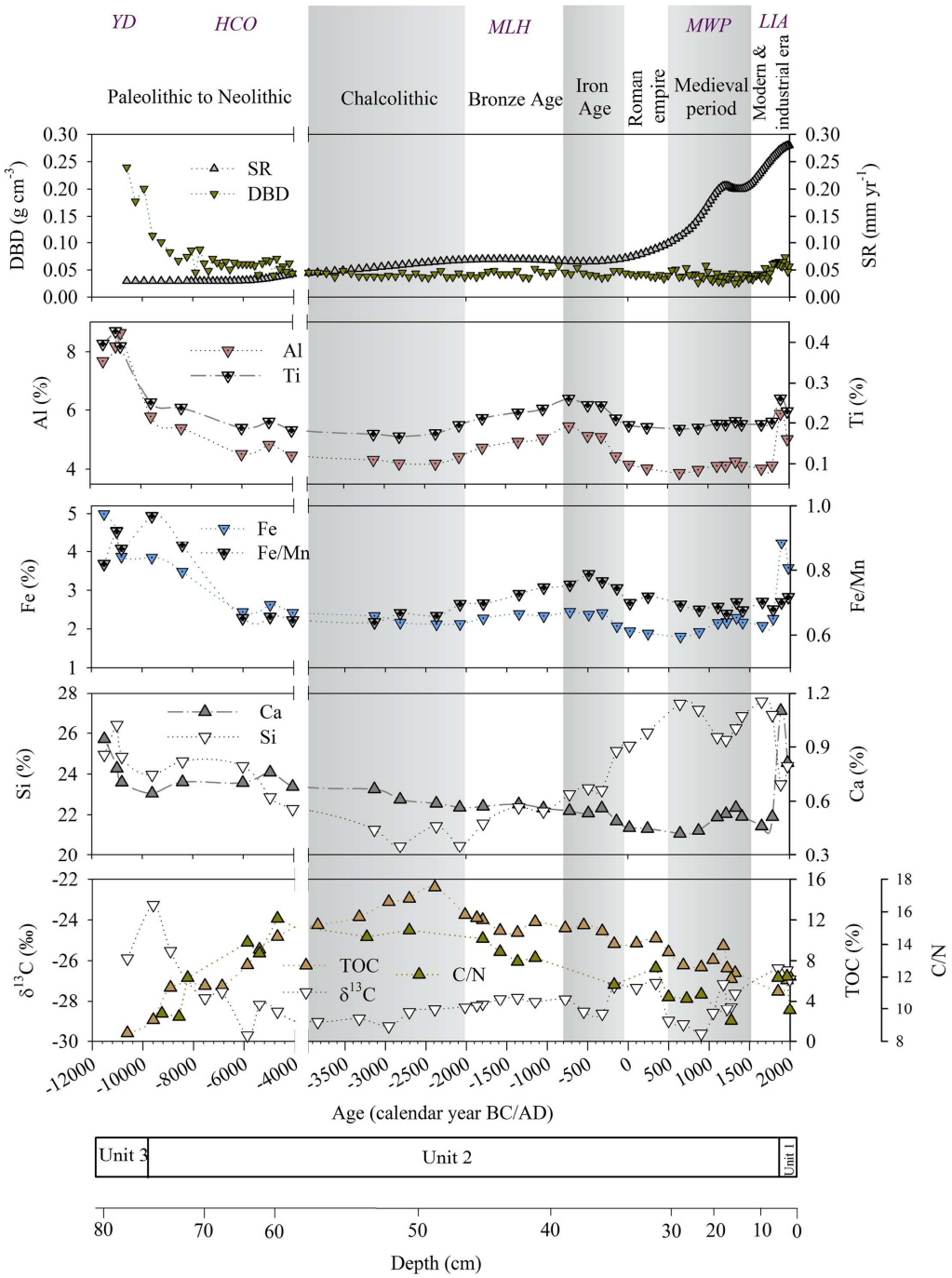

Fig. 3: Dry bulk density (DBD) sedimentation rate (SR), Al, Ti Fe, Mn, Fe/Mn, SiO_2, as a function of age (calendar year AD/BC) in core ROB15-P6. Sediment levels older than 10,800 BC could not be dated and were assigned arbitrary dates.

(YD: Younger Dryas; HCO: Holocene climatic optimum; MLH: middle to late Holocene ; MWP: medieval warm period; LIA: little ice age)

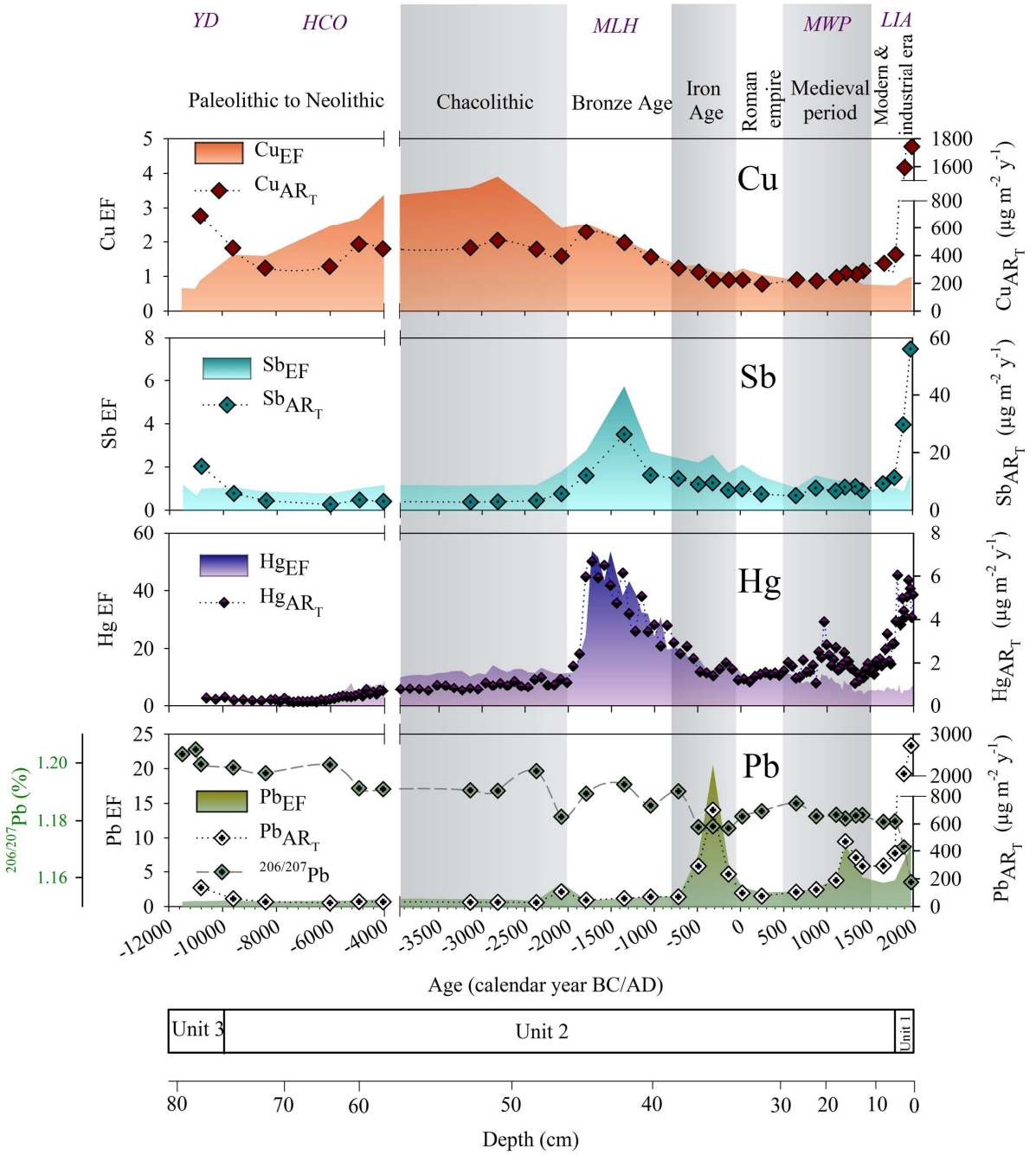

Fig. 4: Enrichment factors (EF) relative to background concentration normalized to Ti, total accumulation rates (AR_T) for Cu, Sb, Hg and Pb, $^{206}Pb/^{207}Pb$ vs calibrated age (AC/DC) in Lake Robert. Sediment levels older than 10,800 cal BC could not be dated and were assigned arbitrary dates.

See text for the calculation of EF.

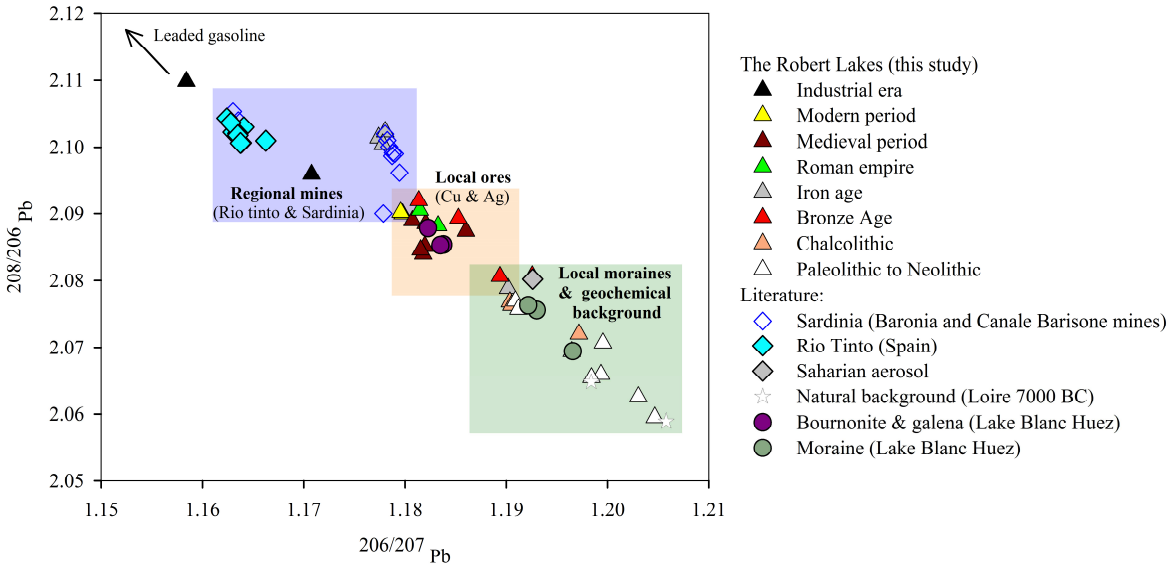

Fig. 5: Plot of $^{206}Pb/^{207}Pb$ ratios vs $^{208}Pb/^{206}Pb$ ratios in Lake Robert and in potential natural and anthropogenic sources. Sources of literature data: Sardinia and Rio Tinto (Oxford archaeological lead isotope database (OXALID) (Stos-Gale and Gale, 2009); Saharan aerosol (Alfonso et al., 2001); natural background (Elbaz-Poulichet et al., 1984); Bournonite, Galena and Moraine (Garçon et al., 2012)

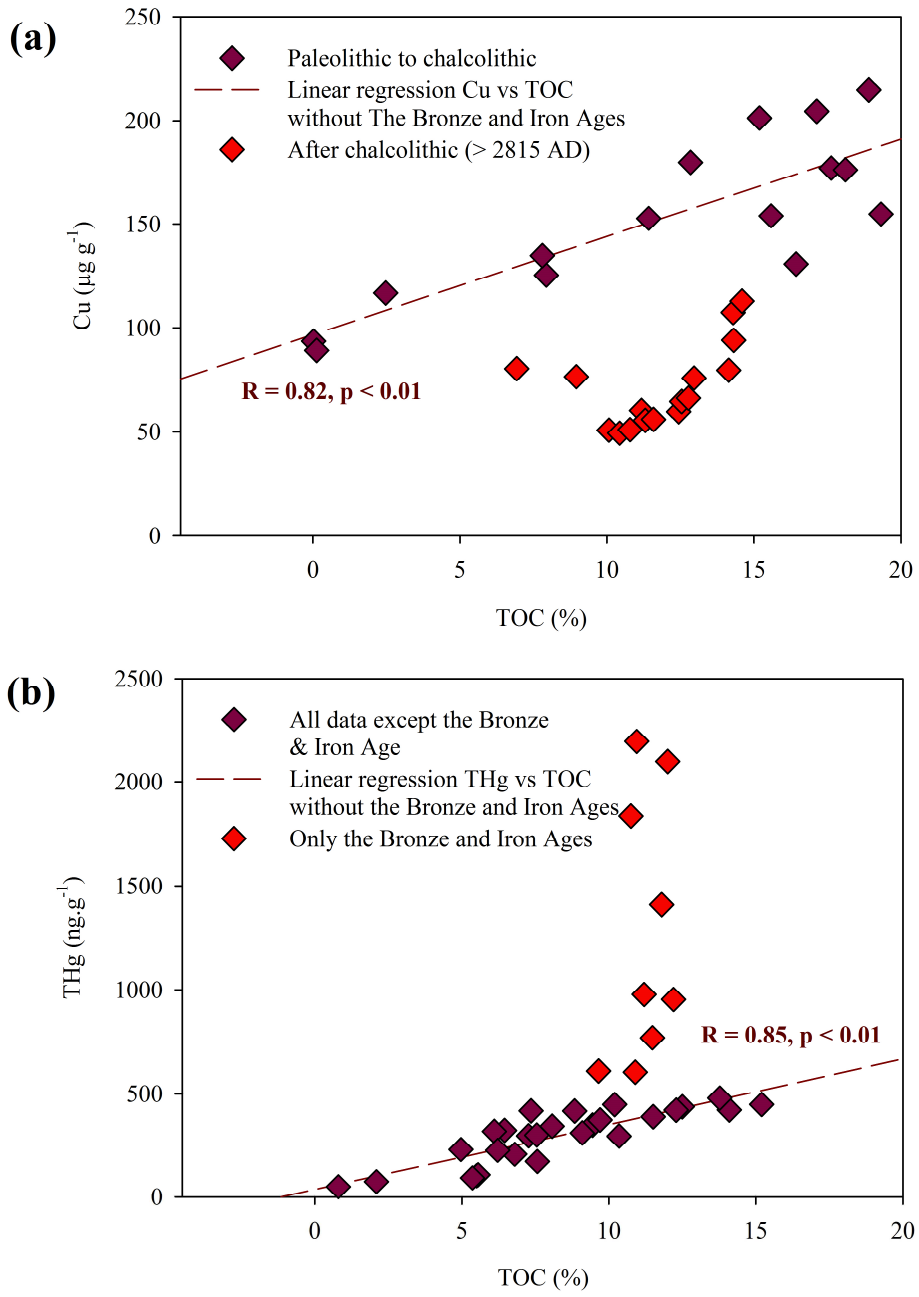

Fig.6: Cu (a) and Total Hg (b) vs TOC

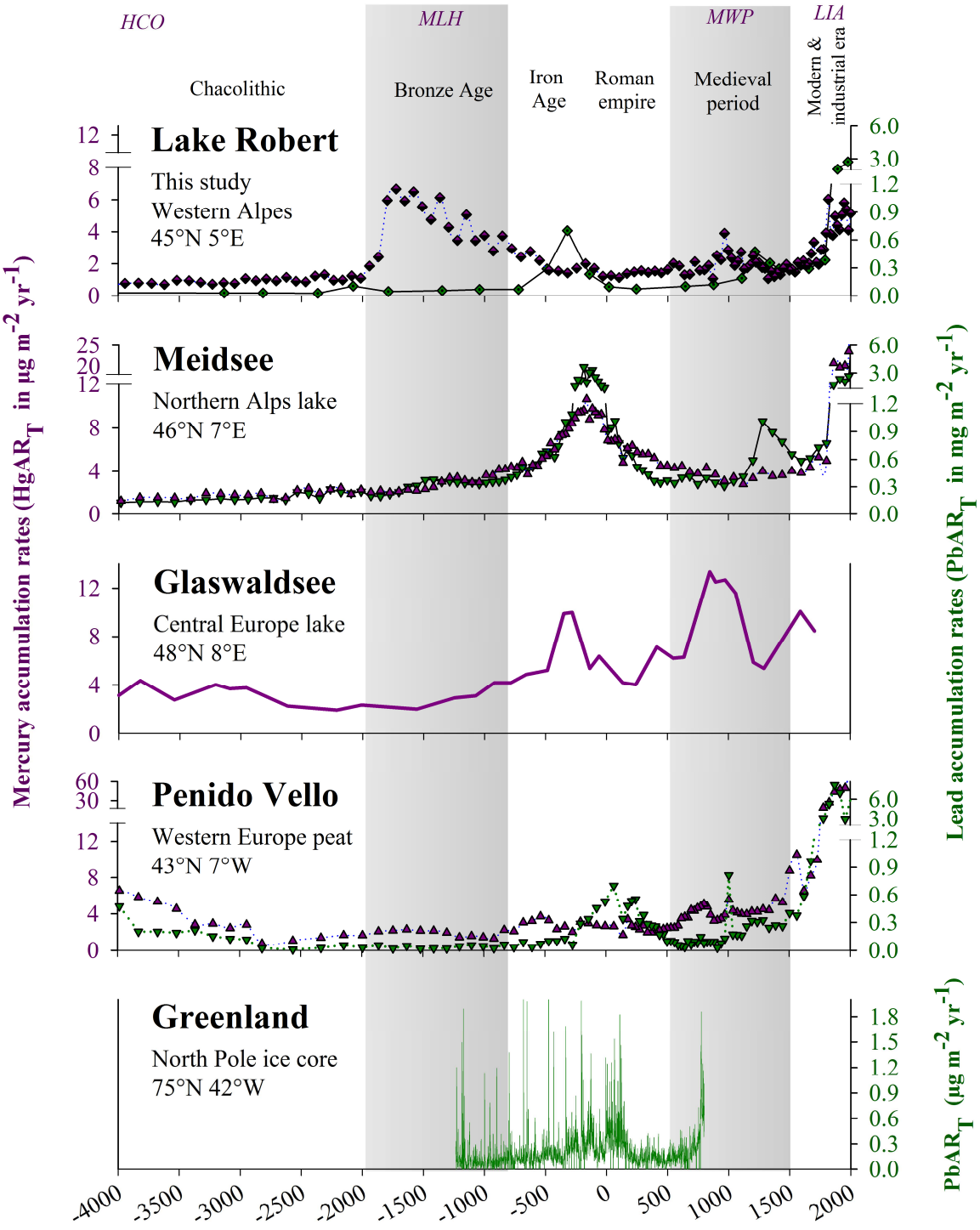

Fig. 7: Pb and Hg AR_T in lake Robert record compared to selected European records: lake Meidsee (Thevenon et al., 2011), Lake Glaswaldsee (Schütze et al., 2018), Penido Vello (Martinez-Cortizas et al., 1999, 1997) and to Greenland Ice record (McConnell et al., 2018)